

MAGE: All- [MASK] Block Already Knows Where to Look in Diffusion LLM

Omin Kwon¹ Yeonjae Kim¹ Doyeon Kim¹ Minseo Kim¹ Yeonhong Park¹ Jae W. Lee¹

Abstract

Block diffusion LLMs are emerging as a promising next paradigm for language generation, but their use of KV caching makes memory access a dominant bottleneck in long-context settings. While dynamic sparse attention has been actively explored, existing methods designed for autoregressive LLMs rely on approximate importance estimation and perform poorly when adapted to block diffusion. This work identifies a key opportunity unique to block diffusion: attention at the first All- [MASK] denoising step reliably predicts important KV entries and budget requirements, enabling MAGE to perform a single exact attention pass per block and reuse it for training-free sparse denoising. Across long-context benchmarks including LongBench and Needle-in-a-Haystack, MAGE achieves near-lossless accuracy with a fraction of the KV budget while delivering up to 3–4× end-to-end speedup, consistently outperforming AR-oriented sparse attention baselines. A lightweight fine-tuning strategy further strengthens [MASK]-guided patterns with minimal cost, requiring only a few hours of training on a single NVIDIA H100 GPU for both 1.5B and 7B models.

1. Introduction

Block diffusion LLMs have emerged as a promising paradigm that combines the benefits of autoregressive (AR) and diffusion-based generation (Arriola et al., 2025; Wu et al., 2025a; Cheng et al., 2025). By generating tokens in a block-wise autoregressive manner while enabling parallel token generation within each block via diffusion, these models achieve competitive accuracy compared to AR models while offering higher throughput. Furthermore, the block-wise generation scheme enables KV caching, which reduces redundant computation and, in long-context settings, often

¹Department of Computer Science and Engineering, Seoul National University, Seoul, South Korea. Correspondence to: Jae W. Lee <jaewlee@snu.ac.kr>.

makes memory access a dominant bottleneck as the KV cache grows.

Dynamic sparse attention has proven effective at reducing KV cache memory access in AR LLMs by dynamically estimating and fetching only the important tokens at each decoding step (Tang et al., 2024; Yang et al., 2025b). The same principle can be applied to block diffusion LLMs, performing sparse attention at each denoising forward pass. However, existing methods rely on approximate importance estimation, such as reusing one layer’s selection across other layers (Yang et al., 2025b) or estimating token importance from page-level representative values (Tang et al., 2024), and achieve only 36–82% top-K recall rate when adapted to block diffusion (Figure 10).

We observe that block diffusion LLMs present a unique opportunity for higher-fidelity sparse attention that does not exist in AR LLMs. The attention patterns computed on the initial All- [MASK] block, the first denoising step where all positions contain [MASK] tokens, reliably predict the important KV positions for all subsequent denoising steps. Specifically, the top-K indices selected from the All- [MASK] block maintain 84–90% recall rate throughout the entire denoising process (Figure 1), far exceeding the recall achieved by existing methods. Furthermore, the relative budget requirements across layers remain stable from the initial All- [MASK] state to the fully decoded state, enabling reliable layer-adaptive budget allocation.

Based on these observations, we propose MAGE ([MASK]-Guided Sparse Attention), a dynamic sparse attention method tailored for block diffusion LLMs. MAGE uses the attention computed on the All- [MASK] block to identify critical KV positions with layer-adaptive budgets, then reuses these positions for all subsequent denoising steps. By leveraging this temporal consistency unique to block diffusion, MAGE achieves substantially higher recall than existing sparse attention methods, maintaining near-lossless accuracy while effectively reducing KV cache memory access for significant end-to-end speedup.

While MAGE works effectively without any training, we further propose a lightweight fine-tuning framework that strengthens the model’s reliance on [MASK]-guided attention patterns. With less than 200 training steps, the fine-tuned model often surpasses even exact attention per-

formance, as the model learns to concentrate its attention more consistently around the patterns established by the All- [MASK] block.

We evaluate MAGE on various subtasks in LongBench. MAGE achieves comparable accuracy to exact attention even at small budgets such as $K=512$ and 1024 , where Quest and Tidal still show significant degradation. In terms of latency, MAGE delivers up to $3\text{--}4\times$ end-to-end speedup over the dense attention baseline while preserving accuracy, demonstrating that the memory access reduction translates directly into practical wall-clock gains.

With fine-tuning, MAGE further improves accuracy: at the same sparse budget, the fine-tuned model matches or exceeds exact attention accuracy on 4 out of 6 subtasks, and surpasses the dense attention baseline on several of them. This suggests that the concentrated attention patterns learned through [MASK]-guided fine-tuning act as an implicit regularizer, improving generation quality beyond what dense attention achieves.

Our contributions are summarized as follows:

- We analyze attention patterns in block diffusion LLMs and discover that the All- [MASK] block provides reliable guidance for sparse attention throughout the denoising process: (1) top-K indices maintain 84–90% recall rate, and (2) layer-wise budget requirements remain stable across denoising steps.
- We propose MAGE, a training-free dynamic sparse attention method that leverages All- [MASK]-guided selection to achieve 84–90% top-K recall, substantially outperforming existing methods such as Quest (48–82%) and Tidal (36–74%) adapted to block diffusion.
- We introduce a lightweight fine-tuning framework that strengthens [MASK]-guided patterns with minimal cost (100 200 steps, less than 10 hours for Fast-dLLM 7B on a single H100), often surpassing dense attention performance.
- We demonstrate $3\text{--}4\times$ end-to-end speedup over exact attention on long-context benchmarks while maintaining comparable accuracy, significantly outperforming existing sparse attention methods at the same budget.

2. Background

2.1. Diffusion LLMs

Diffusion LLMs have emerged as a new paradigm for language generation, breaking the left-to-right sequential dependency of autoregressive (AR) models and enabling multiple token updates per step (Gong et al., 2023; 2025). Among various formulations, diffusion LLMs such as LLaDA (Nie

et al., 2025) and Dream (Ye et al., 2025a) have recently become a standard approach, generating text by iteratively denoising sequences of [MASK] tokens. These models typically employ iterative denoising strategies that either denoise a static number of tokens per step based on confidence or entropy (Kim et al., 2025a), or adaptively vary the denoising set size via thresholding-based selection (Wu et al., 2025b). However, initial masked diffusion models are computationally inefficient in practice, as their bidirectional attention is incompatible with standard KV caching mechanisms (Kim et al., 2025b). They also exhibit suboptimal task performance compared to strong AR baselines (Nie et al., 2025; Ye et al., 2025a).

More recently, Block Diffusion LLMs have emerged as a compromise architecture between AR and diffusion-based generation (Arriola et al., 2025). These models follow a block-wise autoregressive decoding scheme while enabling parallel token generation within each block via diffusion. Notably, block diffusion models achieve competitive accuracy compared to state-of-the-art AR models while offering higher throughput due to parallelism. In this work, we focus on Block Diffusion LLMs, as they represent the most practical and performant diffusion-based paradigm.

2.2. Acceleration of Diffusion LLMs

Fully bidirectional diffusion LLMs recompute the entire sequence at every denoising step, making decoding largely compute-bound. To address this inefficiency, prior work has explored approximation-based acceleration methods. Some approaches divide the sequence into blocks and cache approximate representations for inactive blocks, recomputing only one active block at a time (Wu et al., 2025a; Cheng et al., 2025). Others identify reusable sparse attention patterns to approximate full attention computation (Wang et al., 2025b). While these methods can be applied on-the-fly at inference time, they inevitably introduce approximation errors that may accumulate across denoising steps.

More recent work converts bidirectional diffusion models into block diffusion models (Wang et al., 2025a; Kim et al., 2025c), while others adapt pretrained AR models such as Qwen (Yang et al., 2025a) into block diffusion models (Wu et al., 2025a; Cheng et al., 2025). These methods enable exact, block-level KV caching without approximation, shifting the primary bottleneck from computation to memory access under modest block sizes (e.g., 32 or fewer). As a result, the efficiency of block diffusion models becomes increasingly dominated by KV cache memory access, particularly in long-context scenarios where the cache size grows substantially. Our method directly targets this memory bottleneck by introducing sparse attention tailored for Block Diffusion LLMs.

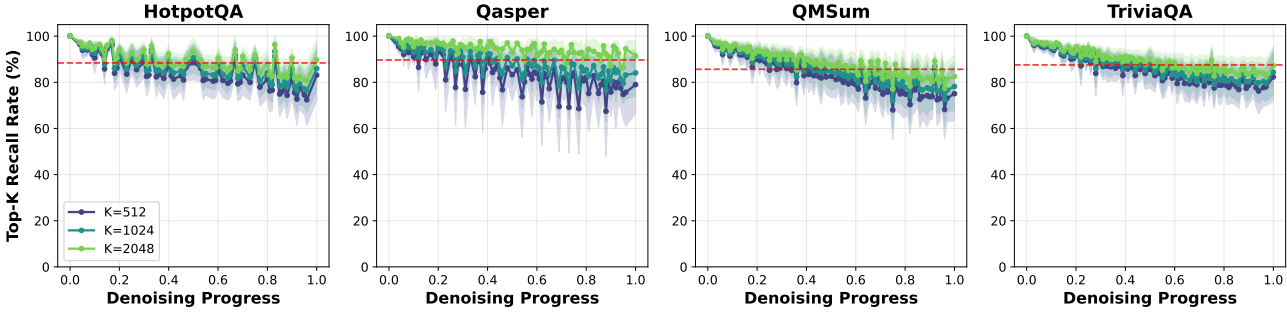


Figure 1. Top-K recall rate across denoising steps on LongBench tasks (0: All- [MASK] block, 1: fully decoded block). The top-K indices selected from the All- [MASK] block maintain 84–90% recall throughout denoising.

2.3. Dynamic Sparse Attention in Autoregressive LLMs

Dynamic sparse attention techniques are widely used in AR decoding to reduce memory access by dynamically selecting a small subset of the KV cache to attend to. Xiao et al. (2024) attends to attention sink tokens and the most recent context using a sliding window, while other works estimate token importance at each decoding step via approximation to avoid full attention computation (Tang et al., 2024; Yang et al., 2025b). Yang et al. (2025c) further extends dynamic sparse attention to modern GQA architectures (Ainslie et al., 2023) by sharing selections across attention heads. In addition, several works observe that different layers and attention heads require different selection budgets for effective sparse attention. PyramidKV (Cai et al., 2024) addresses this by using a predefined, layer-wise budget schedule, while other approaches infer budgets dynamically from prefill-stage signals (Tu et al., 2025) or by sampling a small number of tokens (Feng et al., 2025; Zhu et al., 2025; Lin et al., 2025).

3. All- [MASK] Block Already Knows

In this section, we present a key observation that enables effective and efficient dynamic sparse attention for block diffusion LLMs. We find that the attention scores computed at the first denoising step, namely on the All- [MASK] block, already contains the signal needed to guide sparse attention throughout the subsequent denoising steps. Specifically, two pieces of information demonstrate temporal consistency across denoising steps within a block: (1) the top-K KV entries, and (2) attention score skewness.

3.1. Consistent Top-K KV Entries

Each block begins as an All- [MASK] block and generates tokens through multiple denoising steps. At each step t , we compute the oracle top-K set $S_{\text{oracle}}^{(t)}$ via full attention. To measure how well the initial selection remains valid, we define the top-K recall rate at step t as $|S_{\text{oracle}}^{(0)} \cap S_{\text{oracle}}^{(t)}|/K$: the fraction of step-0 selections that remain in the oracle set at step t . Figure 1 shows the top-K recall across

denoising steps on four LongBench tasks. As denoising progresses, the recall gradually decreases but remains consistently high, with average values of 83.8% for $K=512$, 86.2% for $K=1024$, and 89.6% for $K=2048$. These results indicate that the important context identified at the All- [MASK] step is largely preserved across denoising steps, enabling the All- [MASK] block to serve as a reliable guide for sparse attention in subsequent steps.

For comparison, we evaluate two representative sparse attention methods designed for AR LLMs, Quest (Tang et al., 2024) and Tidal (Yang et al., 2025b), adapted to block diffusion. We measure each method’s top-K recall as $|S_{\text{method}} \cap S_{\text{oracle}}|/K$, where S_{method} denotes the method’s selected set and S_{oracle} is the oracle set from full attention. As shown in Figure 10, Quest achieves 48–82% recall via page-level importance estimation, while Tidal achieves 36–74% by reusing anchor layer selections across other layers. All- [MASK]-guided selection achieves substantially higher recall (84–90%) by leveraging the temporal consistency of attention patterns unique to block diffusion. Intuitively, this consistency arises because the All- [MASK] block, despite lacking decoded token information, already captures the structural relevance patterns of the input context.

3.2. Consistent Attention Score Skewness

For dynamic sparse attention, determining how many KV entries to select in each layer is as important as identifying which KV entries are important. Layers exhibit different levels of attention-score skewness. Under a fixed total computation budget, it is beneficial to select fewer KV entries to more skewed layers and more KV entries to less skewed layers. Importantly, each layer’s skewness remains highly stable across denoising steps within a block.

Figure 2 visualizes the temporal consistency of layer-wise skewness within a block. As a proxy for skewness, we measure, for each layer, the number of KV entries required to reach 90% attention coverage (the cumulative sum of attention scores after softmax), averaged over KV heads.

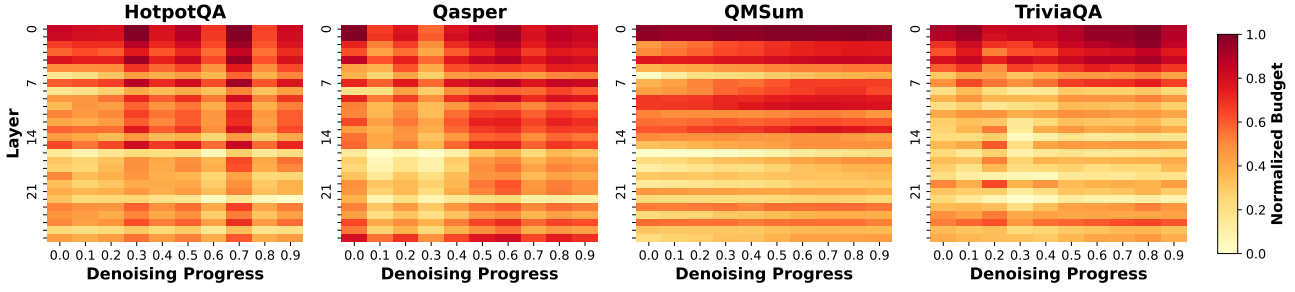


Figure 2. Layer-wise budget across denoising progress on four LongBench tasks. Color indicates normalized budget (darker = higher). Early layers require larger budgets, while horizontal bands indicate stable relative budgets throughout denoising.

Algorithm 1 MAGE Inference

```

Require: KV cache  $\mathcal{C}$ , block size  $B$ , budget  $K$ , steps  $T$ 
Ensure: Generated block  $\mathbf{x}$ 
1: Initialize block with  $B$  [MASK] tokens
2: // Phase 1: Exact Attention with Union Formation ( $t = 1$ )
3: for each layer  $\ell \geq 2$  do
4:    $\mathbf{A}_\ell \leftarrow \text{Softmax}(\mathbf{Q}_{\text{MASK}} \mathbf{K}^\top / \sqrt{d})$ 
5:   for each KV head  $h$  do
6:      $\mathcal{T}_q \leftarrow \text{TopK}(\mathbf{A}_\ell[q, :], K)$  for each query  $q$ 
7:      $\mathcal{U}_h \leftarrow \bigcup_q \mathcal{T}_q$  {Union via voting}
8:      $p_h \leftarrow \frac{1}{GB} \sum_q \sum_{i \in \mathcal{U}_h} \mathbf{A}_\ell[q, i]$  {Coverage}
9:   end for
10:   $s_\ell \leftarrow \max_h |\mathcal{U}_h| \cdot (1 - \log p_h)$  {Adjusted score}
11: end for
12: // Phase 2: Index Selection
13: for each layer  $\ell$ , each KV head  $h$  do
14:    $K^\ell \leftarrow \max \left( K_{\min}, \lfloor \frac{s_\ell}{\sum_{\ell'} s_{\ell'}} \cdot K \cdot L \rfloor \right)$ 
15:    $\mathbf{T}_{\ell, h} \leftarrow \text{SelectTopK}(\mathcal{U}_h, K^\ell)$  {From union}
16: end for
17: // Phase 3: Sparse Denoising ( $t = 2$  to  $T$ )
18: for  $t = 2$  to  $T$  do
19:   for each layer  $\ell \geq 2$  do
20:      $\mathbf{o}_\ell \leftarrow \text{SparseAttn}(\mathbf{Q}, \mathcal{C}[\mathbf{T}_\ell])$ 
21:   end for
22:   Unmask high-confidence positions
23: end for
24:  $\mathcal{C} \leftarrow \mathcal{C} \parallel \text{KV}(\mathbf{x})$  {Update KV cache}
25: return  $\mathbf{x}$ 

```

Although skewness varies substantially across layers and tasks, it remains largely stable across denoising steps, as indicated by the horizontal band-like patterns in each heatmap. This stability suggests that skewness measured at the first denoising step can be reused to allocate layer-specific budgets throughout the entire denoising process.

4. MAGE: [MASK]-Guided Sparse Attention

Based on the observations in Section 3, we propose MAGE ([MASK]-Guided Sparse Attention), a dynamic sparse attention method that uses the attention scores computed on the first denoising step’s All-[MASK] block to guide the remaining steps of block generation.

4.1. MAGE Inference

Algorithm 1 presents the complete MAGE inference procedure. For each block, the first denoising step computes exact attention on the All- [MASK] block and selects critical KV indices with layer-adaptive budgets. All subsequent steps reuse these selected indices for sparse attention.

Phase 1: Exact Attention with Union Formation. In the first denoising step, we compute exact attention between the All- [MASK] block and all preceding KV cache, obtaining the attention matrix \mathbf{A}_ℓ for each layer ℓ . For each query q , we select its local top- K indices based on the attention scores. These selections are aggregated across all $G \times B$ queries sharing each KV head h by taking their union, forming a head-specific set \mathcal{U}_h that covers the top- K indices of all queries. To quantify attention coverage for each KV head, we compute the coverage p_h , the average attention probability captured by the union:

$$p_h = \frac{1}{GB} \sum_q \sum_{i \in \mathcal{U}_h} \mathbf{A}[q, i] \quad (1)$$

Not all layers require the same number of KV entries: layers where attention is concentrated on a few positions can operate with a smaller allocation, while layers with dispersed attention need more. To estimate each layer’s demand, we define an *adjusted score* $s_{\ell, h}$ per KV head that combines union size with attention coverage:

$$s_{\ell, h} = |\mathcal{U}_h| \cdot (1 - \log p_h) \quad (2)$$

A larger union or lower coverage both increase the score, indicating that the head requires more KV entries. We take the maximum across heads as the layer’s adjusted score $s_\ell = \max_h s_{\ell, h}$, since all heads within a layer share the same allocation in practice for memory access efficiency.

Phase 2: Layer-Adaptive Allocation and Selection.

Given a target budget K per layer on average, MAGE distributes the total budget $K \times L$ proportionally based on

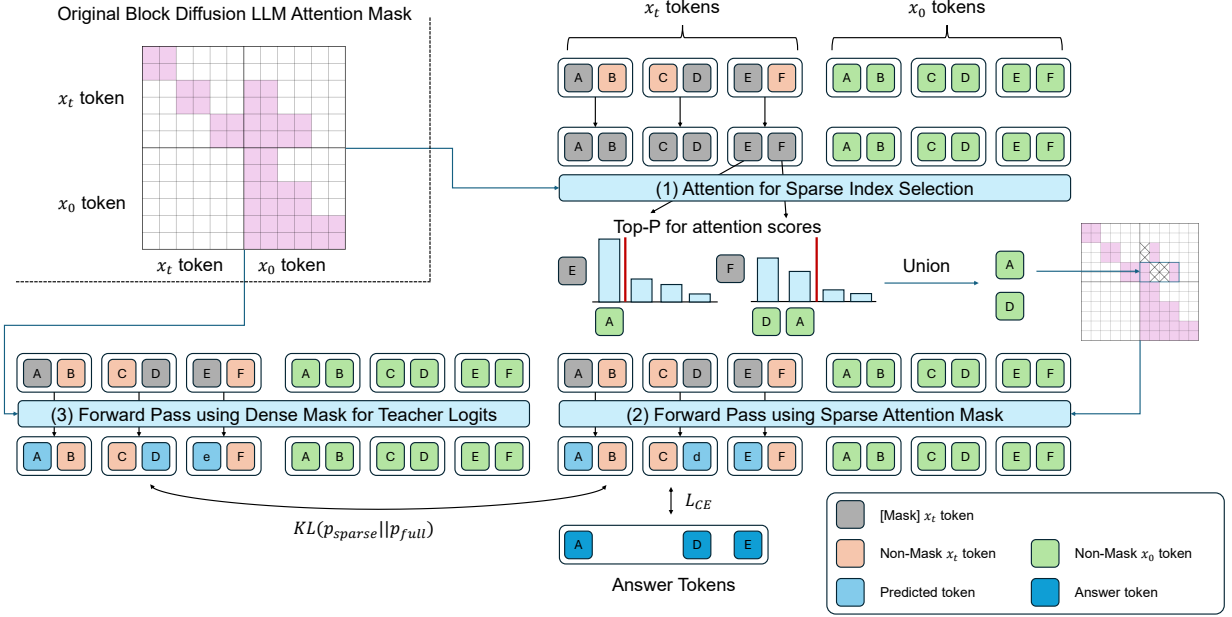


Figure 3. Overview of the MAGE Fine-tuning process. The process consists of three stages: (1) Index Selection identifies important KV indices via Top-K selection without gradients; (2) Sparse Forward applies the sparse mask and computes gradients; (3) Teacher Forward provides exact reference logits for self-distillation.

adjusted scores:

$$K^\ell = \max \left(K_{\min}, \left\lfloor \frac{s_\ell}{\sum_{\ell'} s_{\ell'}} \cdot K \cdot L \right\rfloor \right) \quad (3)$$

where K_{\min} ensures a minimum allocation per layer. Each KV head constructs its final index set $\mathbf{T}_{\ell,h}$ by selecting top- K^ℓ indices from the union based on voting scores. If the allocation exceeds the union size, the entire union is included and remaining slots are filled with recent KV positions. Notably, since index selection for layer ℓ depends only on statistics computed at layer ℓ , it can be overlapped with the exact attention computation of layer $(\ell + 1)$, effectively hiding the overhead. In contrast, Quest must complete importance estimation before attention can proceed, and Tidal requires the previous layer's results, making their overhead unavoidable. We provide detailed latency analysis in Section 5.2.

Phase 3: Sparse Denoising. The selected indices $\mathbf{T}_{\ell,h}$ are cached and reused for all subsequent denoising steps ($t = 2$ to T). At each step, sparse attention retrieves only the KV pairs at these positions, and the model progressively unmasks high-confidence tokens. This reuse is justified by our observation that [MASK]-identified critical positions remain consistent throughout denoising.

4.2. Fine-tuning for Boosting All- [MASK] Block’s Guidance

While MAGE works effectively without training, lightweight fine-tuning can further improve sparse attention accuracy by encouraging the model to more consistently attend to relevant context in the All- [MASK] block state. To achieve this, we design a three-stage training process (Figure 3) that aligns the model with MAGE’s inference scheme. Following Fast-dLLM-v2 (Wu et al., 2025a), we duplicate each training sample into a noisy half x_t , where a subset of tokens in each block is randomly replaced with [MASK] tokens, and a clean half x_0 containing the original uncorrupted text. We apply an offset block-causal mask that restricts queries from x_t to attend only to their corresponding x_0 blocks.

Forward Process. Figure 3 illustrates the three stages. *Stage 1: Sparse Index Selection.* Mirroring MAGE inference, we compute exact attention on the All- [MASK] block (x_t replaced with [MASK] tokens) and select critical KV indices via Top-P on the attention scores. This pass runs without gradient computation. We take the union of selected indices across all query heads sharing the same KV head and cache them for the subsequent stage.

Stage 2: Sparse-Aware Forward. We execute the primary gradient-based forward pass using the cached sparse indices. The sparse mask is applied specifically to the cross-attention region ($x_t \rightarrow x_0$), while self-attention within the context

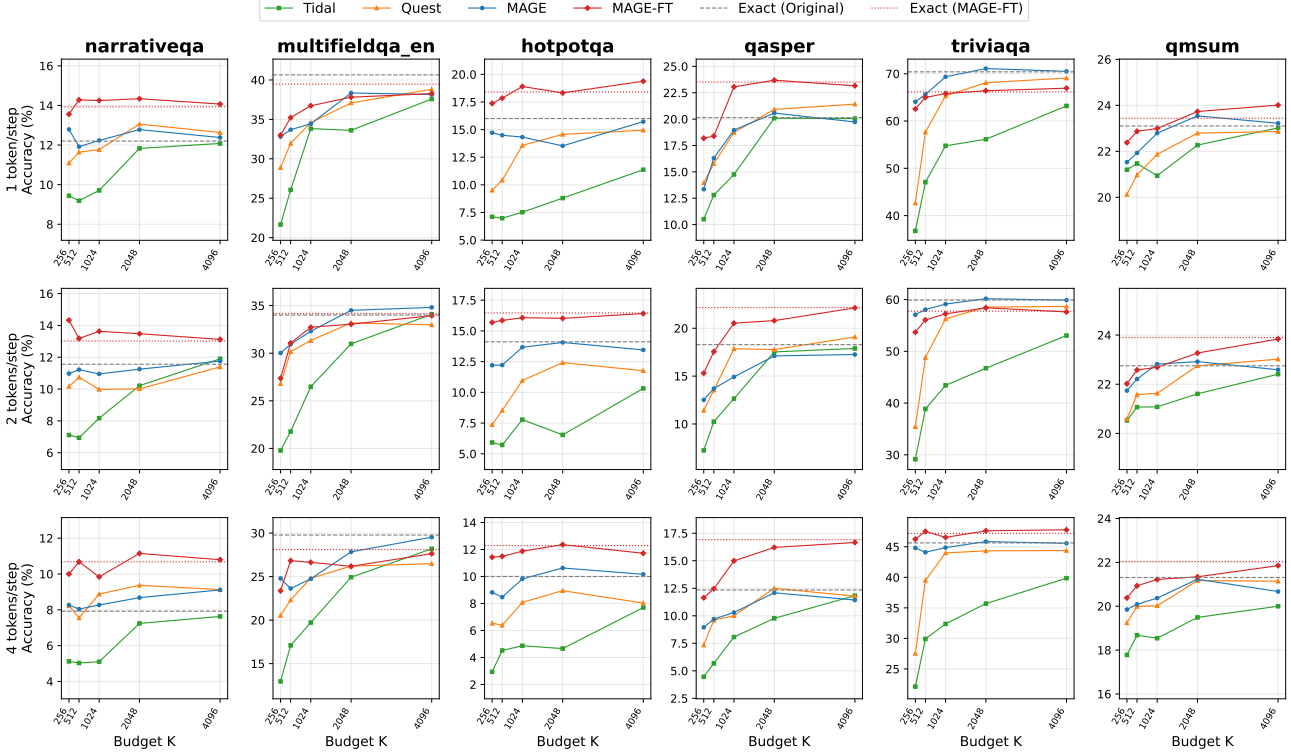


Figure 4. Per-task accuracy on LongBench with Fast-dLLM 1.5B across three denoising configurations (1, 2, 4 tokens/step). MAGE and MAGE-FT consistently outperform Quest and Tidal across all tasks and budgets. MAGE-FT often surpasses exact attention at moderate budgets, while maintaining robustness at higher tokens per step.

$(x_0 \rightarrow x_0)$ and within the noisy block $(x_t \rightarrow x_t)$ remains exact. To ensure training stability, the initial two layers maintain exact attention.

Stage 3: Teacher Forward. We perform an inference-only pass using exact attention to generate reference teacher logits for self-distillation.

Training Objective. We employ self-distillation where the same model serves as both teacher and student. We observe that optimizing with cross-entropy loss alone provides insufficient signal for adapting the model under sparse attention; thus we introduce KL divergence loss to encourage the sparse-constrained model to mimic the exact teacher’s outputs:

$$\mathcal{L} = \mathcal{L}_{\text{CE}} + \lambda \text{KL}(p_{\text{sparse}} \| p_{\text{exact}}) \quad (4)$$

where \mathcal{L}_{CE} is the cross-entropy loss with ground truth tokens, and p_{exact} , p_{sparse} are softmax distributions (with temperature τ) from exact and sparse attention paths respectively. Gradients flow only through p_{sparse} ; the exact path serves as a fixed target.

Fine-tuning Time. Although this scheme requires three forward passes, the overhead is significantly mitigated as

Table 1. Needle-in-a-Haystack accuracy (%). Bold = best sparse method.

	8K Context					32K Context				
	256	512	1K	2K	4K	256	512	1K	2K	4K
<i>Fast-dLLM 7B</i> (Exact: 100 / 88)										
Quest	88	91	100	100	100	27	45	73	73	76
Tidal	85	67	76	82	100	12	27	27	27	61
MAGE	85	94	100	100	100	39	45	61	64	70
<i>Fast-dLLM 1.5B</i> (Exact: 100 / 91)										
Quest	33	64	70	85	97	18	18	24	36	55
Tidal	21	42	67	82	97	12	15	18	24	33
MAGE	48	55	70	91	100	21	30	39	42	42

two passes (Stages 1 and 3) are executed without gradient tracking. Our approach achieves strong sparse accuracy within 200 steps for Fast-dLLM 1.5B and 100 steps for Fast-dLLM 7B on a single NVIDIA H100 GPU.

5. Experiments

Setup. We evaluate two variants of the proposed method: **MAGE** denotes the training-free version that directly leverages All-[MASK] block guidance, while **MAGE-FT** refers to the version further enhanced through our lightweight

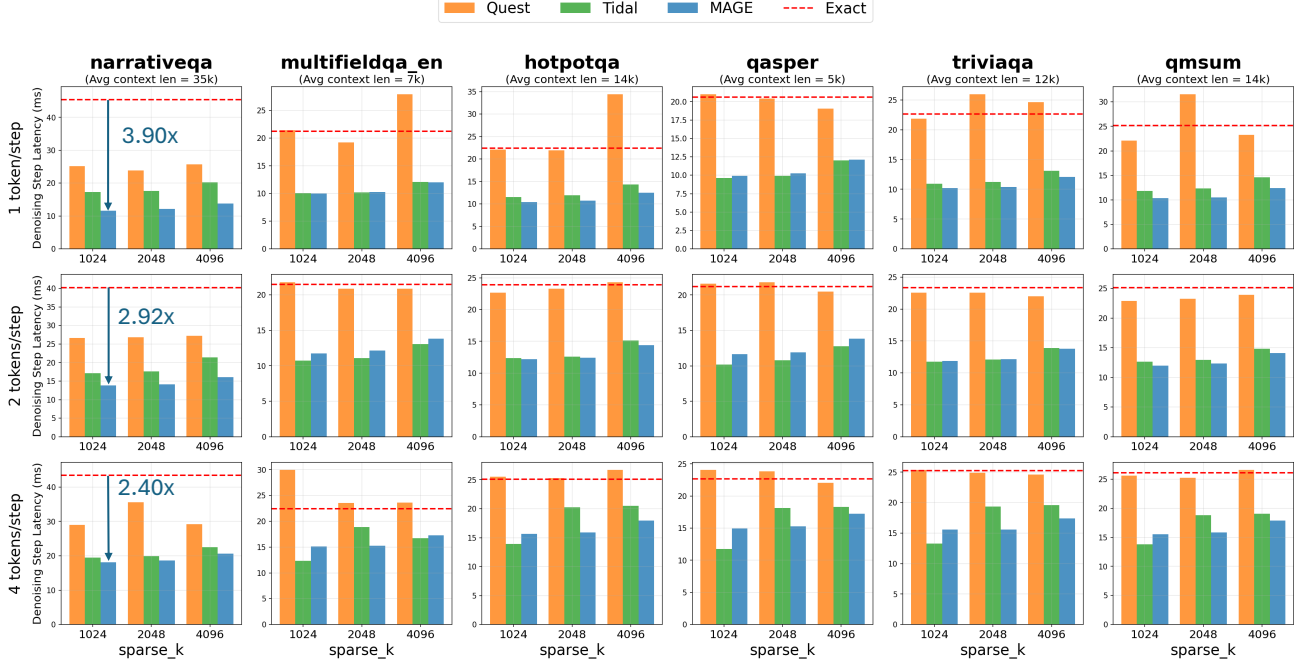


Figure 5. Per-task average denoising step latency on LongBench with Fast-dLLM 1.5B across three denoising configurations (1, 2, 4 tokens/step).

fine-tuning framework. We evaluate our methods on two different scale block diffusion models: Fast-dLLM 1.5B and Fast-dLLM 7B (Wu et al., 2025a). We compare our methods against the exact attention method and two sparse attention methods: Quest (Tang et al., 2024) and Tidal (Yang et al., 2025b).

We fine-tuned Fast-dLLM 1.5B and 7B for inference on a long-context subset from the Daring-Anteater dataset. Specifically, the 1.5B model was trained for 200 steps with a learning rate of 1×10^{-5} and $\lambda = 0.5$, while the 7B model used 100 steps, a learning rate of 5×10^{-6} , and $\lambda = 1.5$, requiring only a few hours on a single NVIDIA H100 GPU. For unmasking, we use the static strategy to control the number of denoising steps and fairly compare the accuracy across all methods. All sparse attention kernels are implemented using FlashInfer (Ye et al., 2025b), and experiments are conducted on NVIDIA H100 GPUs.

5.1. Accuracy Evaluation

LongBench. We evaluate on LongBench (Bai et al., 2024), a comprehensive long-context benchmark, including single-document QA: NarrativeQA, Qasper, MultiFieldQA; multi-document QA: HotpotQA; few-shot learning: TriviaQA; and summarization: QMSum. Budget K ranges from 256 to 4096. We evaluate across three denoising configurations (1, 2, and 4 tokens/step) to examine the speed-accuracy trade-off.

Figure 4 shows results on Fast-dLLM 1.5B. Both MAGE and MAGE-FT consistently outperform Quest and Tidal across all tasks, budgets, and step configurations. This advantage stems from [MASK]-guidance, which enables both high top-K recall rate and layer-adaptive budget allocation (Figure 1). Notably, MAGE achieves near-exact attention performance without any training, demonstrating the effectiveness of our training-free approach.

MAGE-FT further improves upon MAGE, often surpassing exact attention performance at moderate budgets ($K \geq 1024$). This improvement comes from the fine-tuning procedure that strengthens the model’s reliance on [MASK]-guided sparse attention patterns. Through self-distillation, where the exact-attention path serves as the teacher and the sparse-attention path as the student, the model learns to concentrate its attention on the positions selected by MAGE. As a result, the fine-tuned model exhibits a substantially reduced accuracy gap between exact and sparse attention inference.

Needle in a Haystack. We evaluate retrieval capability using the Needle-in-a-Haystack (NIAH) benchmark at 8K and 32K context lengths (Table 1). At 8K context, MAGE matches exact attention (100%) at $K \geq 1024$ on the 7B model and reaches 91% at $K=2048$ on the 1.5B model, while Tidal drops to 67% (7B) and 42% (1.5B) at $K=512$. At the more challenging 32K context, all sparse methods degrade significantly, but MAGE consistently achieves the

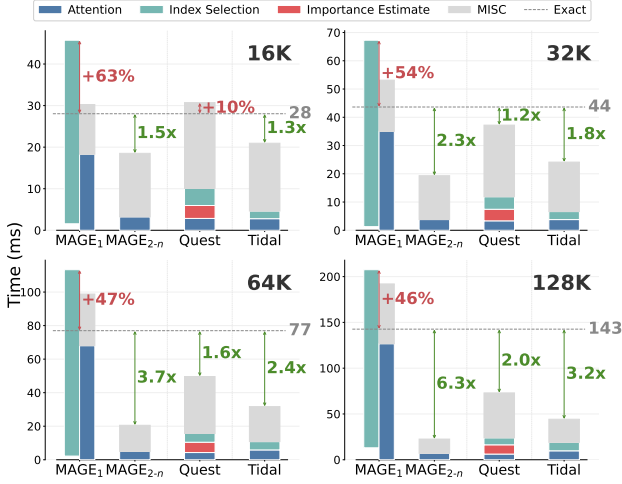


Figure 6. Denoising step latency breakdown from 16K to 128K context length (top- k =2048). For MAGE₁, stacked bars separate overlapped and main-stream operations. Dashed lines indicate exact attention latency. Extended results in Appendix A.4.

highest recall at low budgets ($K \leq 512$) across both models. Tidal degrades most severely, dropping to just 12% at $K=256$ on both model sizes. These results confirm that MAGE’s [MASK]-guided selection preserves critical retrieval capability better than alternatives under aggressive sparsity.

5.2. Efficiency Evaluation

End to End Latency We evaluate the per-step inference latency of MAGE on LongBench (see Figure 5). Per-step latency is defined as the total wall-clock time divided by the number of denoising steps, measured on a single GPU. Compared with exact-attention decoding, MAGE yields substantial per-step speedups that scale with the number of tokens per step: on the 1.5B model, the average speedup increases from $1.66\times$ at 4 tokens/step to $2.01\times$ at 2 tokens/step and $2.37\times$ at 1 token/step; on the 7B model, it grows from $1.48\times$ to $1.70\times$ and $1.81\times$ under the same settings, peaking at $3.92\times$ on NarrativeQA (1.5B, 1 token/step). Among sparse attention baselines, MAGE consistently outperforms Quest in every pairwise comparison, achieving $1.48\text{--}2.15\times$ lower per-step latency on average. Against Tidal, MAGE delivers competitive or superior latency at ≤ 2 tokens/step, winning 75–79% of comparisons at 1 token/step for both model sizes. As illustrated in Figures 4 and 8, MAGE consistently outperforms other sparse attention methods in accuracy within the same computational budget, while maintaining highly competitive inference speeds.

Denoising Steps Breakdown Figure 6 shows the latency breakdown of a single denoising step across context lengths from 16K to 128K with top- k =2048. We classify all sparse

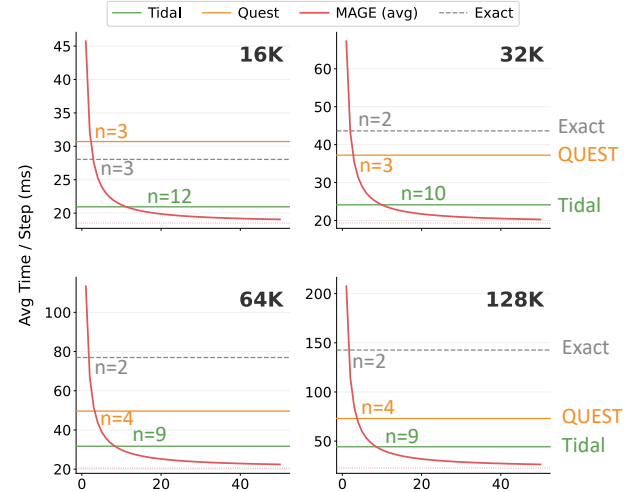


Figure 7. Amortization of first-step overhead ($K=2048$). Dashed lines: baseline per-step latency. Labels: break-even step count.

index computation overhead, including importance estimation and top- k filtering, under Index Selection. In the first denoising step (MAGE₁), our method incurs 46–63% overhead compared to exact attention due to importance estimation, but multi-stream execution effectively overlaps this with attention computation. In subsequent steps (MAGE_{2-n}), our method achieves significant speedups: $1.5\times$ at 16K, $2.3\times$ at 32K, $3.7\times$ at 64K, and $6.3\times$ at 128K, consistently outperforming both Quest (1.1–2.0 \times) and Tidal (1.3–3.2 \times). This scaling behavior is expected: as context length grows, the KV cache access becomes increasingly memory-bound, making the reduction from sparse attention more impactful.

Amortization of First-Step Overhead. As shown above, MAGE₁ incurs additional overhead due to exact attention for importance estimation. However, this cost is a one-time investment that benefits all subsequent denoising steps. Figure 7 illustrates how this overhead is amortized as the number of denoising steps increases. The labels (e.g., $n=9$) denote the break-even point where MAGE becomes faster than each baseline. At shorter context lengths (16K), MAGE requires 12 steps to outperform Quest and 3 steps for Tidal. As context length increases, the break-even point decreases: at 128K, MAGE outperforms Tidal after only 2 steps and Quest after 4 steps. This trend arises because the first-step overhead ratio decreases with context length (from 63% at 16K to 46% at 128K), while per-step sparse savings scale proportionally. As a result, the break-even point drops to as few as 2 steps, and the overhead is amortized well within a single block’s denoising process.

6. Conclusion

We present MAGE, a [MASK]-guided dynamic sparse attention method for block diffusion LLMs, motivated by the observation that attention computed at the first All-[MASK] block reliably predicts both the important top- K KV entries and stable layer-wise budget needs throughout block denoising. Across LongBench and Needle-in-a-Haystack, MAGE achieves near-lossless accuracy at substantially smaller KV budgets than AR-oriented baselines (Quest, Tidal) adapted to block diffusion, while delivering end-to-end speedups that grow with context length. Finally, a lightweight fine-tuning scheme aligned with MAGE’s inference further strengthens [MASK]-guided patterns with only a few hundred steps on a single H100, often matching or surpassing exact attention at moderate budgets.

Impact Statement

This paper presents work whose goal is to advance the field of machine learning. There are many potential societal consequences of our work, none of which we feel must be specifically highlighted here.

References

Ainslie, J., Lee-Thorp, J., de Jong, M., Zemlyanskiy, Y., Lebrón, F., and Sanghai, S. Gqa: Training generalized multi-query transformer models from multi-head checkpoints. In *Proceedings of the 2023 Conference on Empirical Methods in Natural Language Processing*, 2023.

Arriola, M., Gokaslan, A., Chiu, J. T., Yang, Z., Qi, Z., Han, J., Sahoo, S. S., and Kuleshov, V. Block diffusion: Interpolating between autoregressive and diffusion language models. In *International Conference on Learning Representations*, 2025. URL <https://arxiv.org/abs/2503.09573>.

Bai, Y., Lv, X., Zhang, J., Lyu, H., Tang, J., Huang, Z., Du, Z., Liu, X., Zeng, A., Hou, L., Dong, Y., Tang, J., and Li, J. Longbench: A bilingual, multitask benchmark for long context understanding, 2024. URL <https://arxiv.org/abs/2308.14508>.

Cai, Z., Zhang, Y., Gao, B., Liu, Y., Li, Y., Liu, T., Lu, K., Xiong, W., Dong, Y., Hu, J., and Xiao, W. Pyramidkv: Dynamic kv cache compression based on pyramidal information funneling. *arXiv preprint arXiv:2406.02069*, 2024.

Cheng, S., Bian, Y., Liu, D., Zhang, L., Yao, Q., Tian, Z., Wang, W., Guo, Q., Chen, K., Qi, B., and Zhou, B. Sdar: A synergistic diffusion-autoregression paradigm for scalable sequence generation. *arXiv preprint arXiv:2510.06303*, 2025.

Feng, Y., Lv, J., Cao, Y., Xie, X., and Zhou, S. K. Adakv: Optimizing kv cache eviction by adaptive budget allocation for efficient llm inference. In *Advances in Neural Information Processing Systems*, 2025.

Gong, S., Li, M., Feng, J., Wu, Z., and Kong, L. Diffuseq: Sequence to sequence text generation with diffusion models. In *International Conference on Learning Representations*, 2023. URL <https://openreview.net/forum?id=D8DUDJQKZg>.

Gong, S., Agarwal, S., Zhang, Y., Ye, J., Zheng, L., Li, M., An, C., Zhao, P., Bi, W., Peng, H., Han, J., and Kong, L. Scaling diffusion language models via adaptation from autoregressive models. In *Proceedings of the 2025 International Conference on Learning Representations (ICLR)*, 2025. URL <https://arxiv.org/abs/2410.17891>.

Kim, J., Shah, K., Kontonis, V., Kakade, S., and Chen, S. Train for the worst, plan for the best: Understanding token ordering in masked diffusions. In *Proceedings of the 42nd International Conference on Machine Learning*, 2025a.

Kim, M., Hooper, C., Tomar, A., Xu, C., Farajtabar, M., Mahoney, M. W., Keutzer, K., and Gholami, A. Beyond next-token prediction: A performance characterization of diffusion versus autoregressive language models. *arXiv preprint arXiv:2510.04146*, 2025b. URL <https://arxiv.org/abs/2510.04146>.

Kim, M., Xu, C., Hooper, C., Singh, H., Athiwaratkun, B., Zhang, C., Keutzer, K., and Gholami, A. Cdml: Consistency diffusion language models for faster sampling. *arXiv preprint arXiv:2511.19269*, 2025c. URL <https://arxiv.org/abs/2511.19269>.

Lin, C., Tang, J., Yang, S., Wang, H., Tang, T., Tian, B., Stoica, I., Han, S., and Gao, M. Twilight: Adaptive attention sparsity with hierarchical top-p pruning. *arXiv preprint arXiv:2502.02770*, 2025.

Nie, S., Zhu, F., You, Z., Zhang, X., Ou, J., Hu, J., Zhou, J., Lin, Y., Wen, J.-R., and Li, C. Large language diffusion models. *arXiv preprint arXiv:2502.09992*, 2025. URL <https://arxiv.org/abs/2502.09992>.

Tang, J., Zhao, Y., Zhu, K., Xiao, G., Kasikci, B., and Han, S. Quest: Query-aware sparsity for efficient long-context llm inference. In *Proceedings of the 41st International Conference on Machine Learning*, pp. 47901–47911, 2024.

Tu, D., Vashchilenko, D., Lu, Y., and Xu, P. Vl-cache: Sparsity and modality-aware kv cache compression for vision-language model inference acceleration. In *International Conference on Learning Representations*, 2025.

Wang, X., Xu, C., Jin, Y., Jin, J., Zhang, H., and Deng, Z. Diffusion llms can do faster-than-ar inference via discrete diffusion forcing. *arXiv preprint arXiv:2508.09192*, 2025a. URL <https://arxiv.org/abs/2508.09192>.

Wang, Z., Fang, G., Ma, X., Yang, X., and Wang, X. Sparsed: Sparse attention for diffusion language models. *arXiv preprint arXiv:2509.24014*, 2025b.

Wu, C., Zhang, H., Xue, S., Diao, S., Fu, Y., Liu, Z., Molchanov, P., Luo, P., Han, S., and Xie, E. Fast-dllm v2: Efficient block-diffusion llm, 2025a. URL <https://arxiv.org/abs/2509.26328>.

Wu, C., Zhang, H., Xue, S., Liu, Z., Diao, S., Zhu, L., Luo, P., Han, S., and Xie, E. Fast-dllm: Training-free acceleration of diffusion llm by enabling kv cache and parallel

decoding. *arXiv preprint arXiv:2505.22618*, 2025b. URL <https://arxiv.org/abs/2505.22618>.

Xiao, G., Tian, Y., Chen, B., Han, S., and Lewis, M. Efficient streaming language models with attention sinks. In *International Conference on Learning Representations*, 2024.

Yang, A., Li, A., Yang, B., Zhang, B., Hui, B., Zheng, B., Yu, B., et al. Qwen3 technical report, 2025a. URL <https://arxiv.org/abs/2505.09388>.

Yang, L., Zhang, Z., Chen, Z., Li, Z., and Jia, Z. Tidaldecode: A fast and accurate llm decoding with position persistent sparse attention. In *International Conference on Learning Representations*, 2025b.

Yang, L., Zhang, Z., Jain, A., Cao, S., Yuan, B., Chen, Y., Jia, Z., and Netravali, R. Less is more: Training-free sparse attention with global locality for efficient reasoning. *arXiv preprint arXiv:2508.07101*, 2025c.

Ye, J., Xie, Z., Zheng, L., Gao, J., Wu, Z., Jiang, X., Li, Z., and Kong, L. Dream 7b: Diffusion large language models. *arXiv preprint arXiv:2508.15487*, 2025a. URL <https://arxiv.org/abs/2508.15487>.

Ye, Z., Chen, L., Lai, R., Lin, W., Zhang, Y., Wang, S., Chen, T., Kasikci, B., Grover, V., Krishnamurthy, A., and Ceze, L. Flashinfer: Efficient and customizable attention engine for llm inference serving. *arXiv preprint arXiv:2501.01005*, 2025b.

Zhu, K., Tang, T., Xu, Q., Gu, Y., Zeng, Z., Kadekodi, R., Zhao, L., Li, A., Krishnamurthy, A., and Kasikci, B. Tactic: Adaptive sparse attention with clustering and distribution fitting for long-context llms. *arXiv preprint arXiv:2502.12216*, 2025.

A. Additional Experimental Results

This appendix provides detailed experimental results that supplement the main paper.

A.1. Fast-dLLM-v2-7B Results

Figure 8 presents per-task accuracy results on LongBench for Fast-dLLM 7B. Similar to the 1.5B model results in the main paper, MAGE consistently outperform Quest and Tidal across all tasks and budget settings.

Figure 9 presents per-task per-step latency results on LongBench for Fast-dLLM 7B.

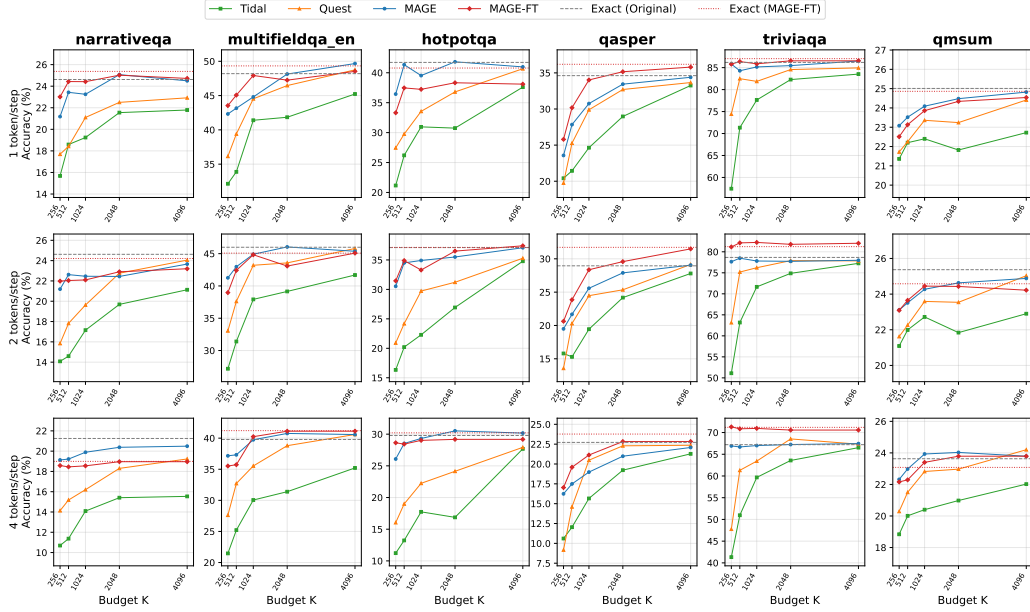


Figure 8. Per-task accuracy on LongBench with Fast-dLLM 7B across varying budget K .

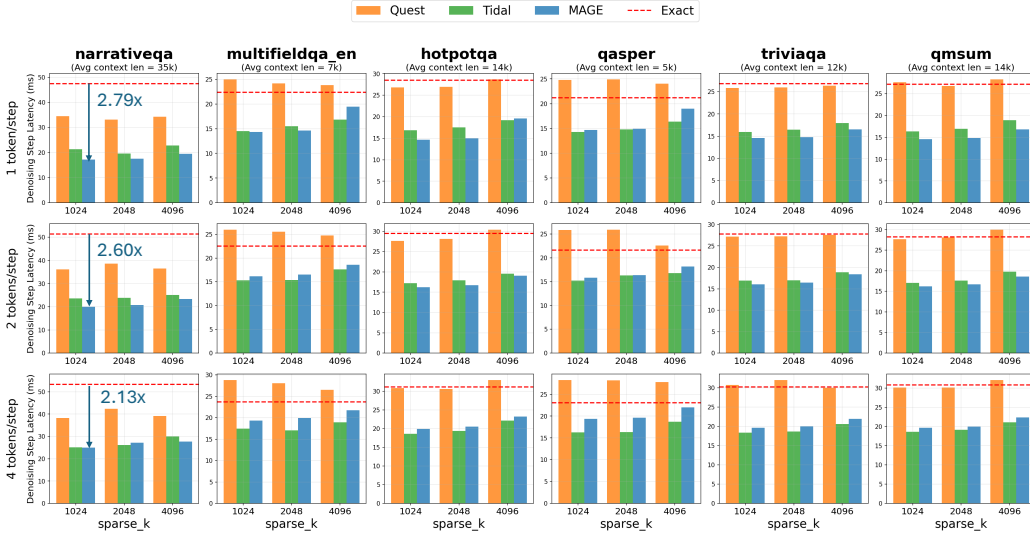


Figure 9. Per-task average denoising step latency on LongBench with Fast-dLLM 7B across three denoising configurations (1, 2, 4 tokens/step).

A.2. Baseline Sparse Attention Methods’ Top-K Recall Rate

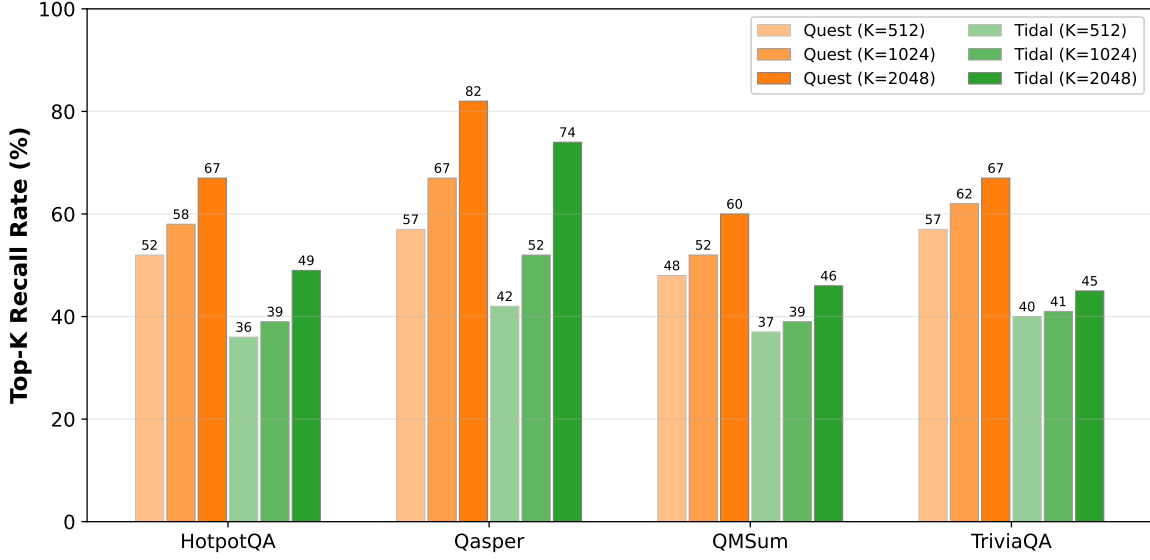


Figure 10. Top-K recall rate of different sparse attention strategies adapted to block diffusion. Quest (48–82%) and Tidal (36–74%) achieve limited recall, while All- [MASK] -guided selection maintains 84–90%.

A.3. Ablation Study: Layer-Adaptive Budget Redistribution

Tables 2 present ablation results comparing MAGE (step reuse only) and MAGE+ (with layer-adaptive budget redistribution). Values show MAGE+ accuracy with the difference from MAGE in parentheses. **Blue (+)** indicates improvement from layer-adaptive budgets, while **red (-)** indicates degradation.

Overall, layer-adaptive budget redistribution provides modest improvements on average, particularly benefiting retrieval-heavy tasks like HotpotQA.

Table 2. Effect of layer-adaptive budget redistribution (32 denoising steps). Values show MAGE+ accuracy with difference from MAGE in parentheses.

Fast-dLLM 1.5B					
Task	256	512	1K	2K	4K
NarrativeQA	12.8 (+0.4)	11.9 (-0.6)	12.2 (+0.2)	12.8 (-0.6)	12.4 (+0.4)
MultiFieldQA	32.8 (-0.2)	33.7 (+0.7)	34.4 (-1.9)	38.4 (+0.1)	38.2 (+0.2)
HotpotQA	14.7 (-0.4)	14.5 (+0.3)	14.3 (+0.9)	13.5 (-0.9)	15.7 (+0.2)
Qasper	13.3 (+0.1)	16.3 (-0.3)	19.0 (+0.9)	20.6 (+0.3)	19.7 (-0.7)
TriviaQA	64.1 (+1.0)	65.6 (+0.2)	69.3 (+1.6)	71.1 (+0.7)	70.5 (+0.4)
QMSum	21.5 (-0.3)	21.9 (-0.2)	22.8 (+0.1)	23.5 (+0.4)	23.2 (+0.2)
Fast-dLLM 7B					
Task	256	512	1K	2K	4K
NarrativeQA	21.2 (+0.3)	23.4 (+0.0)	23.2 (-0.7)	25.1 (-0.8)	24.5 (-0.8)
MultiFieldQA	42.3 (+1.1)	43.2 (+0.3)	44.8 (-1.2)	48.1 (+0.2)	49.7 (+0.1)
HotpotQA	36.4 (+0.3)	41.4 (+1.6)	39.5 (+1.0)	41.8 (+1.8)	41.0 (+0.9)
Qasper	23.6 (-0.9)	27.8 (+1.8)	30.8 (+0.1)	33.4 (+0.1)	34.4 (+0.3)
TriviaQA	85.8 (+0.4)	84.3 (+0.0)	85.2 (-0.2)	85.5 (-0.1)	86.5 (-0.2)
QMSum	23.1 (-0.4)	23.5 (+0.2)	24.1 (+0.0)	24.5 (+0.4)	24.8 (+0.3)

A.4. Extended Breakdown Analysis

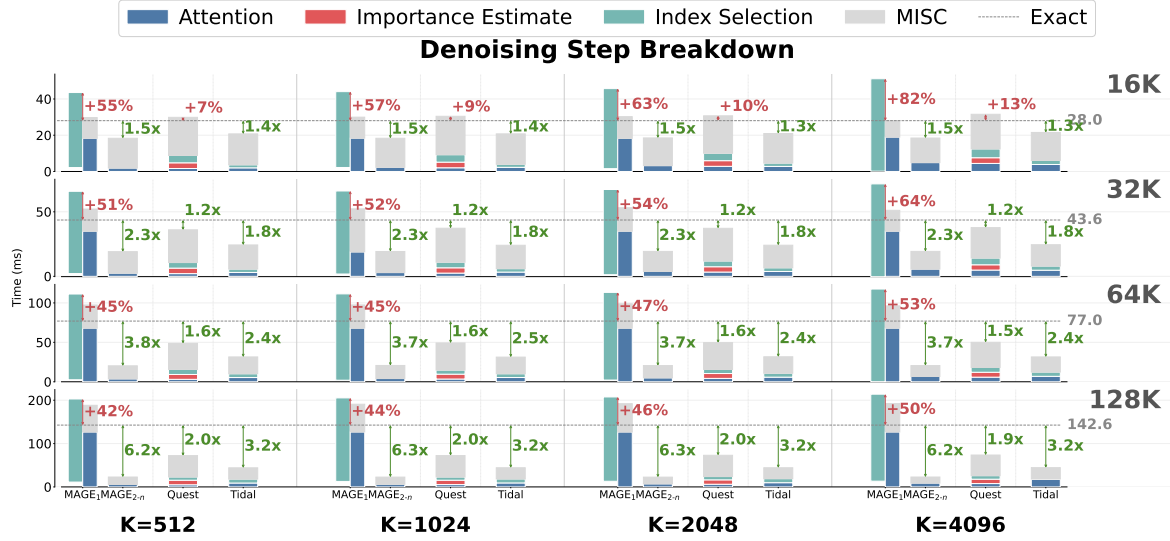


Figure 11. Complete denoising step latency breakdown across context lengths (16K–128K) and top- k values (512, 1024, 2048, 4096). Each group compares Exact attention, Quest, TidalDecode, and MAGE (first step MAGE₁ and subsequent steps MAGE_{2-n}). For MAGE₁, stacked bars show overlapped (left) and main-stream (right) operations. Dashed lines indicate exact attention latency as baseline; numbers denote relative speedup ($>1\times$) or overhead ($<1\times$).

Figure 11 extends the breakdown analysis from Section 5.2 across all K configurations. We observe consistent trends across different K values:

B. Implementation Details

This section describes the optimization techniques employed to achieve efficient sparse attention in Block Diffusion LLMs. All optimizations are applied uniformly across all baseline methods to ensure fair comparison.

B.1. Sparse Attention Kernel Optimization

We build our sparse attention kernel by extending the implementations from TidalDecode (Yang et al., 2025b) and Quest (Tang et al., 2024), which utilize FlashInfer (Ye et al., 2025b) for paged KV cache management with indirect indexing.

The original implementations target autoregressive (AR) decoding, where the query sequence length is always one. To support Block Diffusion models that process multiple query tokens simultaneously, we extend the prefill kernel with the following modifications:

- **Fixed query length support:** The original decode kernels only support query length of one. We extend them to support power-of-two query lengths (e.g., 8, 16, 32) used in block-parallel decoding.
- **GQA-compatible sparse attention:** We modify the kernel to allow each KV head group to access different sparse indices, enabling sparse attention with Grouped-Query Attention (GQA).

B.2. Fused Kernel for Union Formation

When the KV cache length becomes large, even simple operations such as `reshape` and `copy` incur significant overhead due to memory movement. To minimize these costs, we design fused Triton kernels for the Union Formation operation described in Section 4.

Since the tensor shapes remain constant across decoding steps, we exploit this property to pre-compile specialized kernels that:

- Eliminate intermediate memory allocations

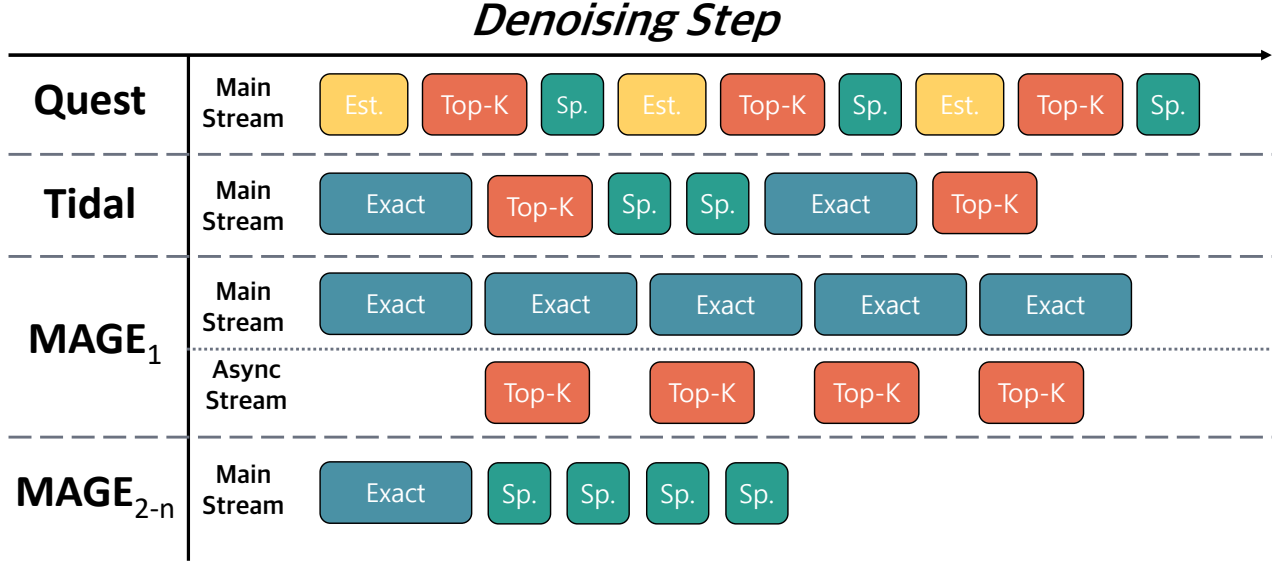


Figure 12. Comparison of attention scheduling strategies within a single denoising step. Quest alternates between importance estimation (Est.) and sparse (Sp.) attention phases. Tidal interleaves exact and sparse attention sequentially. MAGE₁ (first step) performs exact attention on the main stream while asynchronously computing Top-K indices for subsequent steps. MAGE_{2-n} leverages precomputed indices to execute sparse attention, effectively hiding Top-K selection latency through cross-step pipelining.

- Fuse multiple element-wise operations into a single kernel launch
- Minimize memory transactions by operating in-place where possible

B.3. Multi-Stream Execution

In the decoding phase, most operations are memory-bound due to the small batch size. Additionally, our custom attention kernel is configured to use a limited number of streaming multiprocessors (SMs). These characteristics enable effective overlap between independent operations through CUDA streams.

Unlike prior sparse attention methods, our approach allows for extensive pipelining. In TidalDecode, the top- k selection result is immediately required by the next layer, creating a sequential dependency. Similarly, Quest must complete its attention score estimation before performing sparse attention within the same layer. In contrast, our Union Formation and Index Selection operations for a given layer only need to complete before that layer begins in the *next* denoising step, eliminating the intra-step dependency and enabling overlap with the current step’s attention computation.

As illustrated in Figure 12, MAGE₁ computes exact attention while simultaneously preparing Top- k indices on an asynchronous stream, and MAGE_{2-n} directly utilizes these precomputed indices for sparse attention. Specifically, we pipeline the Union Formation and Index Selection operations across multiple CUDA streams. Since these operations do not compete heavily for compute resources, they achieve substantial overlap with the attention computation.

Table 3 demonstrates the effectiveness of multi-stream execution. We measure the overlap benefit as the difference between sequential execution time (Dense + Top- k) and the actual first-step latency. The results show that multi-stream execution reduces the first-step latency by 30–40% compared to sequential execution, with larger savings at longer context lengths. For example, at 128K context with $K=512$, overlap saves 127.17ms out of 330.02ms sequential time (38.5% reduction).

B.4. Reducing Launch Overhead with CUDA Graph

Although Block Diffusion decoding uses longer query sequences than standard autoregressive decoding, the operations remain memory-bound due to the large KV cache size. These memory-bound operations complete quickly on the GPU, making CPU-side kernel launch overhead a significant bottleneck.

To address this, we employ CUDA Graphs to capture and replay the entire decoding step as a single graph execution. This

Table 3. Multi-stream overlap analysis. Each cell shows overlap savings in ms, with total first-step latency in parentheses.

Top- k	16K	32K	64K	128K
512	32.77 (43.56)	41.29 (65.86)	73.62 (111.26)	127.17 (202.85)
1024	32.86 (44.05)	41.81 (66.11)	74.91 (111.43)	126.99 (205.34)
2048	27.26 (45.72)	42.41 (67.27)	74.77 (113.32)	126.65 (207.53)
4096	32.11 (51.16)	46.78 (71.60)	79.69 (117.57)	129.32 (213.91)

eliminates per-kernel launch overhead and reduces CPU-GPU synchronization points, resulting in improved end-to-end latency.

Fair Comparison. All optimization techniques described above—kernel optimization, fused operations, and CUDA Graph—are applied consistently to all baseline methods evaluated in our experiments. This ensures that performance differences reflect algorithmic improvements rather than implementation disparities. Note that multi-stream execution is unique to our method due to the relaxed dependency structure, and thus represents a genuine algorithmic advantage.